Photoinduced reversible phase change in porous molecular crystals based on star-shaped azobenzene tetramers

Massimo Baroncini,*[a] Simone d'Agostino,[a] Giacomo Bergamini,[a] Paola Ceroni,[a] Angiolina Comotti,*[b] Piero Sozzani,[b] Irene Bassanetti,[b] Fabrizia Grepioni,*[a] Taylor M. Hernandez,[a] Serena Silvi,[a] Margherita Venturi[a] and Alberto Credi*[a]

[a] *Dipartimento di Chimica "G. Ciamician", Università di Bologna, via F. Selmi 2, 40126 Bologna, Italy*

[b] *Dipartimento di Scienza dei Materiali, Università di Milano-Bicocca, via R. Cozzi 55, 20125 Milano, Italy*

The development of solid materials that can be reversibly interconverted by light between forms with different physico-chemical properties is of high interest for separation, catalysis, optoelectronics, holography, mechanical actuation, and solar energy conversion. Here we describe a series of shape-persistent azobenzene tetramers that form porous molecular crystals in their *E*-configuration, whose porosity can be tuned by changing the peripheral substitutents on the molecule. Efficient *E*→*Z* photoisomerization of the azobenzene units takes place in the solid state and converts the crystals into a non-porous amorphous phase. Crystallinity and porosity are restored upon *Z*→*E* isomerization promoted by visible light irradiation or heating. We demonstrate that the photoisomerization enables reversible on/off switching of optical properties, such as birefringence, and of the capture of carbon dioxide from the gas phase. The linear design, the structural versatility and the synthetic accessibility make this new family of materials extremely interesting for technological applications.

Photochromic compounds are highly appealing for science and technology because they enable the implementation of light-induced functions within molecular, supramolecular and macromolecular species, biological constructs and bulk materials[1–3]. Azobenzene is one of the most attractive photochromes because of its easy functionalization and its clean, fast and reversible photoisomerization between two isomers (*E* and *Z*) exhibiting some significantly different physico-chemical properties[4]. Current and prospective applications of research on azobenzene photoisomerization include holographic information storage[5], optoelectronic devices[6], magnetic memories,[7] nanomachines,[8] control of chemical reactivity[9,10], responsive surfaces[11,12] and materials,[13,14] energy conversion[15], and drug design[16].

In view of these applications azobenzene photoisomerization in the solid state is attracting much interest, but the relatively large free volume change associated with this reaction[17,18] poses a considerable challenge to its practical realization[19,20]. The $E \rightarrow Z$ photoisomerization of azobenzene derivatives is well documented for azobenzene-containing polymers[21], liquid crystals[11,21–27], thin films[28–30] and crystals at the solid-liquid interface[31], whilst a limited number of examples are reported in porous materials[32–36] (e.g. metal-organic and covalent organic frameworks) and in molecular crystalline forms in which the azobenzene moiety is functionalized with polar substituents[37–39]. Our strategy is based on the use of molecules containing a central node which imparts a star-like 3D arrangement to azobenzene moieties for the fabrication of molecular crystals endowed with permanent porosity capable of promoting the reversible *E*/*Z* isomerization in the solid state. Microporous molecular crystals[40–43] may show substantial advantages in terms of preparation, processability, structural diversification and functional flexibility in comparison with porous metal-organic[44] and covalent[45] frameworks. Moreover, the novel molecular crystals exhibit extrinsic porosity (that is, porosity resulting solely from the solid-state molecular packing) which is relatively uncommon and of challenging design[40–43].

As an embodiment of these concepts we describe the preparation, structure, and reversible photoisomerization in the solid state of porous tetra(azobenzene)methane compounds, consisting of

four azobenzene units covalently linked to a tetrahedral carbon atom. We envisaged that the extended branches of the *E*-azobenzene units and the rigid tetrahedral structure of the molecule could prevent a tightly packed arrangement[46], resulting in a porous crystal structure in which the gained free volume, combined with the occurrence of weak van der Waals interactions, may allow photoswitching of the azobenzene units in the solid state. Additionally, it could be anticipated that the packing interactions could be somehow modulated by changing the bulkiness of the peripheral substituents attached to the *para* position of the azobenzene units.

Compounds E_4-**1a–c** (Fig. 1a) having the four azobenzene units in the *E* configuration, and hydrogen, methyl and *tert*-butyl peripheral substituents, respectively, were synthesized in good yield by Mills coupling of tetra(4-aminophenyl)methane with four equivalents of the appropriately *para*-substituted nitrosobenzene in acetic acid. The products were isolated from the reaction mixture by filtration and easily purified by recrystallization (Figs. S1-S6 in the ESI).

The absorption spectra of E_4-**1a–c** in CH_2Cl_2 (Figs. S14-S16) show the typical features of *E*-azobenzene and are consistent with the presence of four such units, although they do not exactly correspond to the sum of the respective individual spectra. For example, the ππ* band of E_4-**1c** (λ_{max} = 345 nm) is red-shifted by 750 cm^{-1} in comparison with that of the 1,1'-dimethyl-*E*-azobenzene model *E*-**2**, suggesting that the four units are not fully independent from an electronic point of view, possibly because of homoconjugation effects. Irradiation of E_4-**1c** at 365 nm causes the $E \rightarrow Z$ isomerization (Fig. 1b) with an initial quantum yield for azobenzene unit Φ_{EZ} = 0.18 (for *E*-**2**, Φ_{EZ} = 0.17). The fact that isosbestic points in the absorption spectra are not precisely maintained and that the $E \rightarrow Z$ photoisomerization quantum yield decreases throughout the irradiation indicates that the four azobenzene units of **1c** exhibit similar but not identical photophysical and photochemical properties. Nevertheless, the $E \rightarrow Z$ conversion upon exhaustive irradiation at 365 nm in CH_2Cl_2 amounts to >95%. ^{1}H NMR analysis of the photostationary state (PSS) obtained in C_6D_6 under the same conditions shows that the composition is 89% Z_4-**1c**, 6%

E_1Z_3-**1c**, 3% E_2Z_2-**1c**, <1% E_3Z_1-**1c** and <1% starting material, corresponding to an overall $E \rightarrow Z$ conversion of 97%. For the sake of simplicity, hereafter we will refer to the PSS obtained upon 365-nm irradiation of E_4-**1c** in CH_2Cl_2 as Z_4-**1c**. Compounds **1a,b** exhibit a similar behaviour, as reported in the ESI (Figs. S7-S11 and S14-S16).

Structure of the molecular crystalline solids

Compounds E_4-**1a–c** crystallize in the tetragonal system (see Table S2 and Figs. S20-S29). In all solids the tetrahedral node lies on a -4 crystallographic axis, and the four azobenzene units are all mutually related by symmetry. The main structural motif observed in crystalline E_4-**1a–c** is the interlocking of adjacent molecules along the four-fold rotoinversion axes, which run parallel to the crystallographic *c*-axis direction (Fig. 2b). This corresponds to the direction of maximum crystal growth, and is apparent both in the ideal and experimental morphology of the crystals obtained from solution or constituting the deposited thin films (Fig. S31). The "open" molecular geometry determined by the four tetrahedrally arranged *E*-azobenzene units (Fig. 2a) combined with the presence of the bulky substituents, especially *tert*-butyl groups in E_4-**1c**, makes it particularly difficult to achieve an efficient space occupation in the solid state, as evidenced by a packing coefficient value of 0.59.

The molecular piles are placed side-by-side in the crystal, with shape taking control of the self-assembly. The resulting crystal packing (Fig. 2c) is characterized in E_4-**1c** by the presence of empty channels along the *c*-axis direction, with a 10.4 % porosity (calculated as the ratio between the accessible volume by a 1.2 Å probe and the cell volume). A channel-like porosity is also observed, though less pronounced, in E_4-**1b** (8.1%), while for E_4-**1a** the porosity (6.7%) is confined to discrete, non-communicating regions along the pile (Fig. S24). In the case of E_4-**1c**, the shape of the channels responsible for crystal porosity shows the periodic presence of necks (Fig. 2d); this feature is unique to E_4-**1c**. A closer inspection of the structure reveals that the necks along the channels

arise from the terminal *tert*-butyl substituents, while the largest sections of the channels are delimited by benzene moieties (Fig. S32). ^{13}C Magic-angle spinning (MAS) NMR spectra of E_4-**1b** and E_4-**1c** show respectively 10 and 11 resonances, in accordance with the highly symmetric arrangement of the molecule in the crystal structure (Figs. S12-S13). No solvent molecules are observed in the spectra, as independently confirmed by thermogravimetric analysis (Fig. S30).

Solid-state photoreactivity and photoinduced phase transitions

To investigate the photoreactivity in the solid state, powders of E_4-**1a–c** were subjected to 365-nm irradiation for 6 h in an NMR tube. ^{1}H NMR spectroscopic analysis performed on the irradiated solid dissolved in C_6D_6 showed indeed the presence of *Z*-azobenzene units (Fig. S11). Quantitative information on the photoisomerization reaction was obtained from irradiation experiments carried out on dry films of **1a–c** deposited on a quartz slide by spin coating or drop casting from a solution. The X-ray powder diffraction (XRPD) pattern measured on drop casted films of E_4-**1a–c** is superimposable to the pattern calculated on the basis of single crystal data (Fig. 3a and S25-S28), thus indicating that the layer contains crystalline particles. In the following we will describe in detail the properties of **1c**, as compounds **1a,b** exhibit a very similar behaviour (Table S1, Figs. S17-S19 amd S33-S36).

The quality and homogeneity of the spin coated thin films enabled characterization by transmission UV-visible absorption spectroscopy. The absorption spectra of E_4-**1c** (Fig. 3b) and Z_4-**1c** (Fig. 3c) in the solid film are similar to those recorded in solution, and show the typical ππ* (ca. 350 nm) and nπ* (ca. 450 nm) bands of azobenzene.

Irradiation of the E_4-**1c** film at 365 nm brings about spectral changes (Fig. 3b) almost identical to those found in solution, indicating an efficient $E \rightarrow Z$ isomerization. From a comparison of the spectra it can be estimated that at the photostationary state about 35% of the azobenzene unit of **1c** are converted to the *Z* configuration. Conversely, no effect is detected when the same experiment is

performed on a film of *E*-**2**, indicating that the rigid tetrahedral arrangement of the azobenzene moieties is crucial for their photoisomerization in the solid. Exposure of the irradiated sample, or a film of previously prepared Z_4-**1c**, to light of 436 nm causes $Z \rightarrow E$ photoisomerization and a photostationary state enriched in *E*-azobenzene units is obtained (Fig. 3c). The absorption spectrum recorded before any irradiation is fully restored by heating the film at 130 °C for 10 min (Fig. 3bc), indicating that (i) thermal $Z \rightarrow E$ isomerization occurs, (ii) E_4-**1c** is the thermodynamically stable form of **1c** in the solid state, and (iii) the photoreaction is a clean process.

The XRPD pattern obtained after 48 h irradiation of the film still corresponds to the pattern of E_4-**1c,** while the intensity of all peaks decreases and disappear after prolonged irradiation, indicating that the material has become amorphous (Fig. 3a). To gain more insight into the effect of light on solid E_4-**1c** we imaged the crystals with a polarizing optical microscope. The crystals of E_4-**1c** exhibit a significant optical birefringence under cross-polarized light illumination (Fig. 4ab), confirming an ordered arrangement of the molecules in the solid that gives rise to anisotropic crystals. It is important to note that the high yield of $E \rightarrow Z$ photoconversion for crystals of this size implies that the photoisomerization of E_4-**1c** upon irradiation in the 350-360 nm region is not limited to surface layers. Efficient bulk photoisomerization of azobenzene solid crystals is made possible, besides the high inherent photoreactivity of the material, because the $E \rightarrow Z$ conversion causes a decrease in the optical density at the irradiation wavelength (Fig. 3b), thus enabling photons to reach the core of the crystals. To our best knowledge, substantial $E \rightarrow Z$ photoisomerization of azobenzene-containing crystals was described only in two latest reports on azobenzene cyclophanes bearing long alkyl substituents[26,27].

Upon near-UV irradiation of the crystals on the microscope slide, both the crystal morphology (Fig. 4c) and the optical birefringence (Fig. 4d) disappear. Indeed, the crystals appear to be melt and the material assumes the consistency of a viscous liquid (Fig. S35). This observation indicates that the photogenerated material is amorphous, in agreement with XRPD data. Again, control experiments

performed on *E*-**2** crystals do not show light-induced effects. Birefringent crystals are formed upon annealing of the irradiated sample at 160 °C for 20 min as a consequence of *Z*→*E* thermal isomerization (Fig. 4ef). The formation of larger crystals in comparison with starting ones is consistent with crystallization from a melt phase. These findings also rule out the possibility that the transformation observed under UV irradiation is caused by local thermal effects and confirms that the observed phenomenon is in fact an isothermal photoinduced crystal-amophous phase transformation taking place at ambient temperature[22,26,27,47]. The photoinduced amorphisation and thermal recrystallization can be repeated on the same sample without degradation of the material.

A detailed examination of the effect of light on the E_4-**1c** crystals reveals an even more interesting behavior, not observed for previously investigated azobenzene-containing crystals[26,27,47]: exposure to UV light for a short time causes no significant change in morphology but affords a dramatic decrease of the birefringence, which is fully restored by heating (Fig. S37). In other words, the loss of optical anisotropy does not require complete amorphisation of the material. Such an observation supports the view, suggested by the XRPD and optical absorption results discussed above, that crystallinity is substantially maintained upon partial *E*→*Z* isomerization of E_4-**1c**. We hypothesize that *E*→*Z* isomerization in a relatively small population of **1c**, such as that afforded in the initial stages of the irradiation, increases the lattice disorder throughout the entire sample to an extent sufficient to disrupt long-range structural anisotropy, thus causing the loss of optical birefringence[48]. The solid, however, remains mostly ordered and the crystal structure and morphology are not affected, as confirmed by the complete regeneration of the film upon thermal annealing (Fig. S37).

Such a behavior is interesting for optical information storage because the thin film behaves as a one-input ternary switch under threshold control. Irradiation with a light dose below the threshold converts state “0”, crystalline and birefringent, to state “1” which is still crystalline but no longer birefringent. Continued irradiation (that is, exposure to a dose of photons above the threshold)

places the film into state “2” characterized by an amorphous structure. Clean and reversible switching among the three states can be performed by appropriate light and heat stimulation.

Gas adsorption experiments

The microporosity of the molecular crystals was demonstrated by gas adsorption measurements (see Figs. S37-S40). While E_4-**1a** exhibits negligible gas uptake properties, the CO_2 isotherm of E_4-**1c** at 195 K shows a Langmuir type-I profile which reaches the value of 52 cm^3(STP)/g at 1 bar, highlighting the open and accessible free-volume in the compound (Fig. 5a). The maximum CO_2 uptake corresponds to the occupancy of four molecules per unit cell (i.e. 2 molecules per cavity) and is consistent with the empty space as estimated from the crystallographic structure, suggesting a complete filling of the cavities by gas diffusion in the permeable crystal. Similarly, the maximum CO_2 sorption of E_4-**1b** compound results in a full loading of the available space (Fig. 5a, inset). In sharp contrast, the CO_2 adsorption isotherms of Z_4-**1b** and Z_4-**1c** samples obtained by precipitation from UV-irradiated solutions exhibit a negligible CO_2 uptake, demonstrating that the all-*Z* isomers are not porous. However, upon heating, the samples are converted back to the porous forms, as shown in the inset of Fig. 5a. Therefore, a reversible switching between the porous and non porous forms was realized[49], taking advantage of photoirradiation and thermal relaxation of the *E*- and *Z*-azobenzene moieties.

Furthermore, the porosity of the molecular crystals was checked by CO_2 and N_2 adsorption measurements under mild conditions of temperature and up to 10 bar. The maximum CO_2 uptake values of 41 cm^3/g and 32 cm^3/g were found for the E_4-**1c** species at 10 bar and temperatures of 273 and 298 K, respectively (Fig. 5b). The pore size of about 7 Å guarantees an excellent interaction with the gas molecules: in fact, the compound exhibits isosteric heat of adsorption (Q_{st}) equal to 28 kJ/mol, indicating the occurrence of favourable interactions of CO_2 with the aromatic groups exposed to the inner surface of the crystalline channels. Instead, N_2 adsorption experiments

collected at 273 and 298 K for both E_4-**1b** and E_4-**1c** showed very limited uptake values even at high pressures, indicating a low affinity of the absorbent for nitrogen (Figs. 5b and S38). This observation can be exploited for the selective capture of carbon dioxide in a mixture with nitrogen: in fact, IAST calculations indicated a CO_2/N_2 selectivity as high as 80 for the E_4-**1b** compound. It is worth noting that this value exceeds the performances of most molecular crystals endowed with permanent porosity[50]. Collectively, the gas adsorption data support the view that E_4-**1a–c** molecules pack inefficiently with one another because of their rigid star-like shape and the presence of bulky groups at the periphery. These features generate a large free-volume in the crystal which enables the $E \rightarrow Z$ photoconversion in the solid state.

Conclusions

A series of compounds based on a tetra(azobenzene)methane-type moiety with diversified end groups (H, Me or *t*-Bu) has been developed. The star-like shape and rigidity of the molecules prevent a close-packed arrangement in the crystals and promote low density molecular self-assembly, affording porous molecular crystals in which azobenzene $E \rightarrow Z$ photoisomerization occurs in the solid state. The porosity of the crystals increases on increasing the size of the terminal substituents introduced in the four azobenzene units. The porous crystals of E_4-**1b,c** adsorb CO_2 from the gas phase selectively with respect to N_2, whereas the corresponding *Z*-isomers, obtained by light irradiation at room temperature, are not porous; crystallinity and porosity are restored upon $Z \rightarrow E$ isomerization promoted by visible light irradiation or heating. These compounds – in particular **1b,c** – possess a number of valuable features, including synthetic accessibility, solution processability, high photoreactivity and tunability of the physico-chemical properties. Such properties are key requirements for materials apt for technological applications as photoswitchable catalysts and membranes, solid-state photonic switches, substrates for holography and photolithography, and photoresponsive adhesives.

The present study contributes to the design of novel microporous molecular solids in which photoreactive groups can be converted by light to high-energy molecular configurations, as the crystal porosity provides the space required for the photoinduced structural changes. It also paves the way for a better understanding of solid-state photochemical reactions and photoinduced phase transitions. The rare combination of porosity and photoactive moieties opens up intriguing perspectives in the field of responsive materials involving light irradiation, molecular movements and chemical stimuli.

Acknowledgments

This work was supported by MIUR (PRIN 2010CX2TLM “InfoChem” and FIRB 2010RBAP11C58Y “Nanosolar”), Fondazione Cariplo 2012-0921, and the University of Bologna.

Authors contributions

M. B., A. C. and An. C. conceived the project. M. B. and T. M. H. synthesized and characterized the compounds; S. d’A. and F. G. performed crystal growth experiments and X-ray diffraction studies; S. S. and M. B. carried out the spectroscopic, photochemical and microscopy experiments; I. B., An. C. and P. S. performed gas adsorption experiments, solid-state NMR spectra, and preparation and characterization of the polymorphs; G. B., P. C., M. V. and all other authors analyzed the data; A. C. wrote the paper.

Additional information

Supplementary information is available in the online version of the paper. Reprints and permissions information is available online at www.nature.com/reprints. Correspondence and request for materials should be addressed to A.C.

Competing financial interests

The authors declare no competing financial interests.

References

1. Kobatake, S., Takami, S., Muto, H., Ishikawa, T. & Irie, M. Rapid and reversible shape changes of molecular crystals on photoirradiation. *Nature* **446,** 778–781 (2007).

2. Szymanski, W., Beierle, J. M., Kistemaker, H. A. V, Velema, W. A. & Feringa, B. L. Reversible photocontrol of biological systems by the incorporation of molecular photoswitches. *Chem. Rev.* **113,** 6114–6178 (2013).

3. Klajn, R. Spiropyran-based dynamic materials. *Chem. Soc. Rev.* **43,** 148–184 (2014).

4. Bandara, H. M. D. & Burdette, S. C. Photoisomerization in different classes of azobenzene. *Chem. Soc. Rev.* **41,** 1809–1825 (2012).

5. Bruder, F.-K., Hagen, R., Rölle, T., Weiser, M.-S. & Fäcke, T. From the surface to volume: concepts for the next generation of optical-holographic data-storage materials. *Angew. Chem. Int. Ed.* **50,** 4552–4573 (2011).

6. Raimondo, C. *et al.* Optically switchable organic field-effect transistors based on photoresponsive gold nanoparticles blended with poly(3-hexylthiophene). *Proc. Natl. Acad. Sci. U. S. A.* **109,** 12375–12380 (2012).

7. Venkataramani, S. *et al.* Magnetic bistability of molecules in homogeneous solution at room temperature. *Science* **331,** 445–448 (2011).

8. Ragazzon, G., Baroncini, M., Silvi, S., Venturi, M. & Credi, A. Light-powered autonomous and directional molecular motion based on a dissipative self-assembling system. *Nat. Nanotechnol.* in press (2014).

9. Stoll, R. S. & Hecht, S. Artificial light-gated catalyst systems. *Angew. Chem. Int. Ed.* **49,** 5054–5075 (2010).

10. Clever, G. H., Tashiro, S. & Shionoya, M. Light-triggered crystallization of a molecular host-guest complex. *J. Am. Chem. Soc.* **132,** 9973–9975 (2010).

11. Kausar, A., Nagano, H., Ogata, T., Nonaka, T. & Kurihara, S. Photocontrolled translational motion of a microscale solid object on azobenzene-doped liquid-crystalline films. *Angew. Chem. Int. Ed.* **48,** 2144–2147 (2009).

12. Venancio-Marques, A., Barbaud, F. & Baigl, D. Microfluidic mixing triggered by an external LED illumination. *J. Am. Chem. Soc.* **135,** 3218–3223 (2013).

13. Yanai, N. *et al.* Guest-to-host transmission of structural changes for stimuli-responsive adsorption property. *J. Am. Chem. Soc.* **134,** 4501–4504 (2012).

14. Brown, J. W. *et al.* Photophysical pore control in an azobenzene-containing metal–organic framework. *Chem. Sci.* **4,** 2858–2864 (2013).

15. Kucharski, T. J. *et al.* Templated assembly of photoswitches significantly increases the energy-storage capacity of solar thermal fuels. *Nat. Chem.* **6,** 441–447 (2014).

16. Velema, W. a *et al.* Optical control of antibacterial activity. *Nat. Chem.* **5,** 924–928 (2013).

17. Naito, T., Horie, K. & Mita, I. Photochemistry in polymer solids. 11. The effects of the size of reaction groups and the mode of photoisomerization on photochromic reactions in polycarbonate film. *Macromolecules* **24,** 2907–2911 (1991).

18. Evans, R. a *et al.* The generic enhancement of photochromic dye switching speeds in a rigid polymer matrix. *Nat. Mater.* **4,** 249–253 (2005).

19. Tsuda, M. & Kuratani, K. Isomerization of cis-azobenzene in the solid phase. *Bull. Chem. Soc. Jpn.* **37,** 1284–1288 (1964).

20. Bushuyev, O. S., Tomberg, A., Friščić, T. & Barrett, C. J. Shaping crystals with light: crystal-to-crystal isomerization and photomechanical effect in fluorinated azobenzenes. *J. Am. Chem. Soc.* **135,** 12556–12559 (2013).

21. Bléger, D., Yu, Z. & Hecht, S. Toward optomechanics: maximizing the photodeformation of individual molecules. *Chem. Commun.* **47,** 12260–12266 (2011).

22. Lee, S. *et al.* Stimulus-responsive azobenzene supramolecules: fibers, gels, and hollow spheres. *Langmuir* **29,** 5869–5877 (2013).

23. Yu, Y., Maeda, T., Mamiya, J.-I. & Ikeda, T. Photomechanical effects of ferroelectric liquid-crystalline elastomers containing azobenzene chromophores. *Angew. Chem. Int. Ed.* **46,** 881–883 (2007).

24. Norikane, Y., Hirai, Y. & Yoshida, M. Photoinduced isothermal phase transitions of liquid-crystalline macrocyclic azobenzenes. *Chem. Commun.* **47,** 1770–1772 (2011).

25. Akiyama, H. & Yoshida, M. Photochemically reversible liquefaction and solidification of single compounds based on a sugar alcohol scaffold with multi azo-arms. *Adv. Mater.* **24,** 2353–2356 (2012).

26. Uchida, E. *et al.* Control of the orientation and photoinduced phase transitions of macrocyclic azobenzene. *Chem. Eur. J.* **19,** 17391–17397 (2013).

27. Hoshino, M. *et al.* Crystal melting by light: X-ray crystal structure analysis of an azo crystal showing photoinduced crystal-melt transition. *J. Am. Chem. Soc.* **136,** 9158–9164 (2014).

28. Nakano, H., Seki, S. & Kageyama, H. Photoinduced vitrification near the surfaces of single crystals of azobenzene-based molecular materials with glass-forming ability. *Phys. Chem. Chem. Phys.* **12,** 7772–7774 (2010).

29. Yan, X., Wang, F., Zheng, B. & Huang, F. Stimuli-responsive supramolecular polymeric materials. *Chem. Soc. Rev.* **41,** 6042–6065 (2012).

30. Harada, A., Takashima, Y. & Nakahata, M. Supramolecular polymeric materials via cyclodextrin-guest interactions. *Acc. Chem. Res.* **47,** 2128–2140 (2014).

31. Ichimura, K. Reversible photoisomerisability and particle size changes of mill-dispersed azobenzene crystals in water. *Chem. Commun.* **45,** 1496–1498 (2009).

32. Brown, J. W. *et al.* Photophysical pore control in an azobenzene-containing metal–organic framework. *Chem. Sci.* **4,** 2858 (2013).

33. Patel, H. a *et al.* Unprecedented high-temperature CO_2 selectivity in N_2-phobic nanoporous covalent organic polymers. *Nat. Commun.* **4,** 1357 (2013).

34. Lyndon, R. *et al.* Dynamic photo-switching in metal-organic frameworks as a route to low-energy carbon dioxide capture and release. *Angew. Chem. Int. Ed.* **52,** 3695–3698 (2013).

35. Park, J., Sun, L.-B., Chen, Y.-P., Perry, Z. & Zhou, H.-C. Azobenzene-functionalized metal-organic polyhedra for the optically responsive capture and release of guest molecules. *Angew. Chem. Int. Ed.* **53,** 5842–5846 (2014).

36. Patel, H. a *et al.* Directing the structural features of N_2-phobic nanoporous covalent organic polymers for CO_2 capture and separation. *Chem. Eur. J.* **20,** 772–780 (2014).

37. Koshima, H., Ojima, N. & Uchimoto, H. Mechanical motion of azobenzene crystals upon photoirradiation. *J. Am. Chem. Soc.* **131,** 6890–6891 (2009).

38. Koshima, H. & Ojima, N. Photomechanical bending of 4-aminoazobenzene crystals. *Dyes Pigm.* **92,** 798–801 (2012).

39. Bushuyev, O. S., Singleton, T. a & Barrett, C. J. Fast, reversible, and general photomechanical motion in single crystals of various azo compounds using visible light. *Adv. Mater.* **25,** 1796–800 (2013).

40. Holst, J. R., Trewin, A. & Cooper, A. I. Porous organic molecules. *Nat. Chem.* **2,** 915–920 (2010).

41. McKeown, N. B. Nanoporous molecular crystals. *J. Mater. Chem.* **20,** 10588–10597 (2010).

42. Sozzani, P., Bracco, S., Comotti, A., Ferretti, L. & Simonutti, R. Methane and carbon dioxide storage in a porous van der Waals crystal. *Angew. Chem. Int. Ed.* **44,** 1816–1820 (2005).

43. Mastalerz, M. & Oppel, I. M. Rational construction of an extrinsic porous molecular crystal with an extraordinary high specific surface area. *Angew. Chem. Int. Ed.* **51,** 5252–5255 (2012).

44. Zhou, H.-C. & Kitagawa, S. Metal–Organic Frameworks (MOFs). *Chem. Soc. Rev.* **43,** 5415–5418 (2014).

45. Feng, X., Ding, X. & Jiang, D. Covalent organic frameworks. *Chem. Soc. Rev.* **41,** 6010–6022 (2012).

46. Aujard, I. *et al.* Tetrahedral onsager crosses for solubility improvement and crystallization bypass. *J. Am. Chem. Soc.* **123,** 8177–8188 (2001).

47. Norikane, Y., Hirai, Y. & Yoshida, M. Photoinduced isothermal phase transitions of liquid-crystalline macrocyclic azobenzenes. *Chem. Commun.* **47,** 1770–1772 (2011).

48. Palmer, B. a *et al.* X-ray birefringence imaging. *Science* **344,** 1013–1016 (2014).

49. Luo, F. *et al.* Photoswitching CO_2 capture and release in a photochromic diarylethene metal-organic framework. *Angew. Chem. Int. Ed.* **53,** 9298–9301 (2014).

50. Comotti, A. *et al.* Porous dipeptide crystals as selective CO_2 adsorbents: experimental isotherms vs. grand canonical Monte Carlo simulations and MAS NMR spectroscopy. *CrystEngComm* **15,** 1503–1507 (2013).

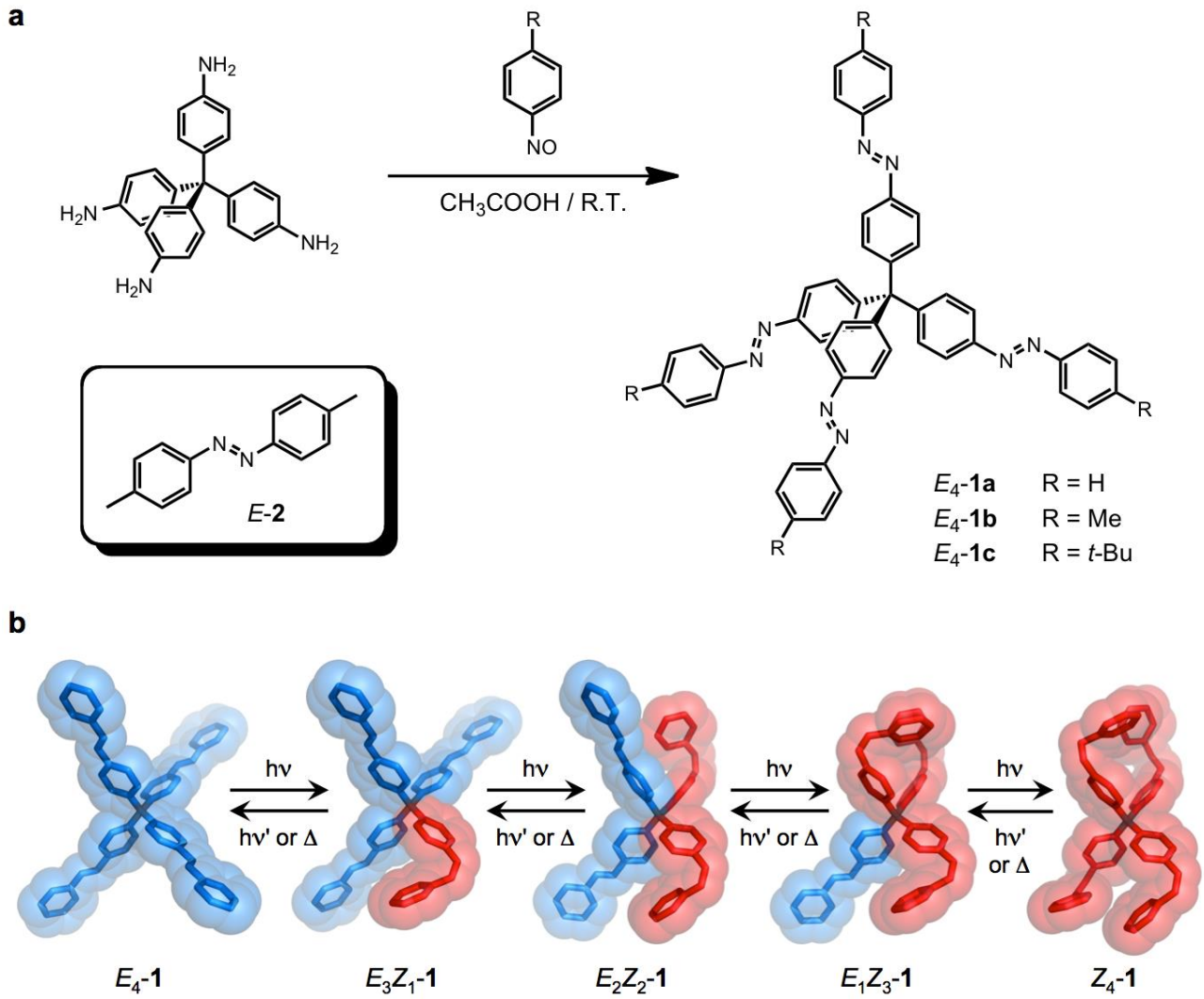

Fig. 1 | Star-shaped azobenzene tetramers and their photochemical transformations. (a) Synthetic route and molecular formula of E_4-**1a–c** and of model compound *E*-**2**. (b) MM3 Optimized molecular structure of the interconverting *E/Z* stereoisomers of **1**. *E*- and *Z*-azobenzene units are colored in blue and red, respectively; peripheral substituents and hydrogen atoms are omitted for clarity.

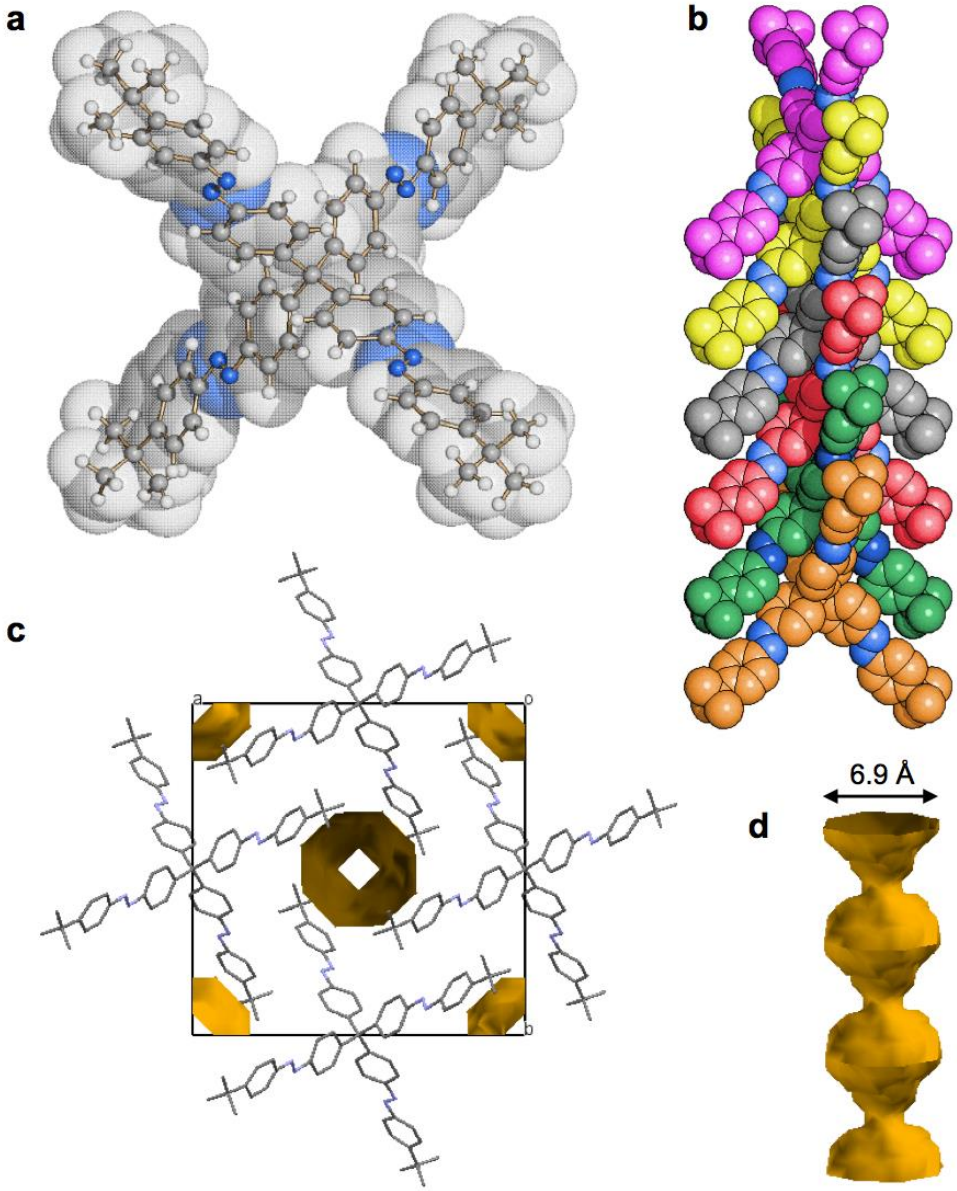

Fig. 2 | Structural properties of E_4-1c in the crystalline state. (a) Molecular structure of E_4-**1c** as observed in its crystals. The four azobenzene units are all equivalent by symmetry. (b) Interlocking of adjacent molecules along the *c*-axis direction (H atoms omitted for clarity). (c) Relative arrangement of molecular piles in crystalline E_4-**1c** and representation of the empty channels extending along the *c*-axis direction. (d) Side view of a channel portion.

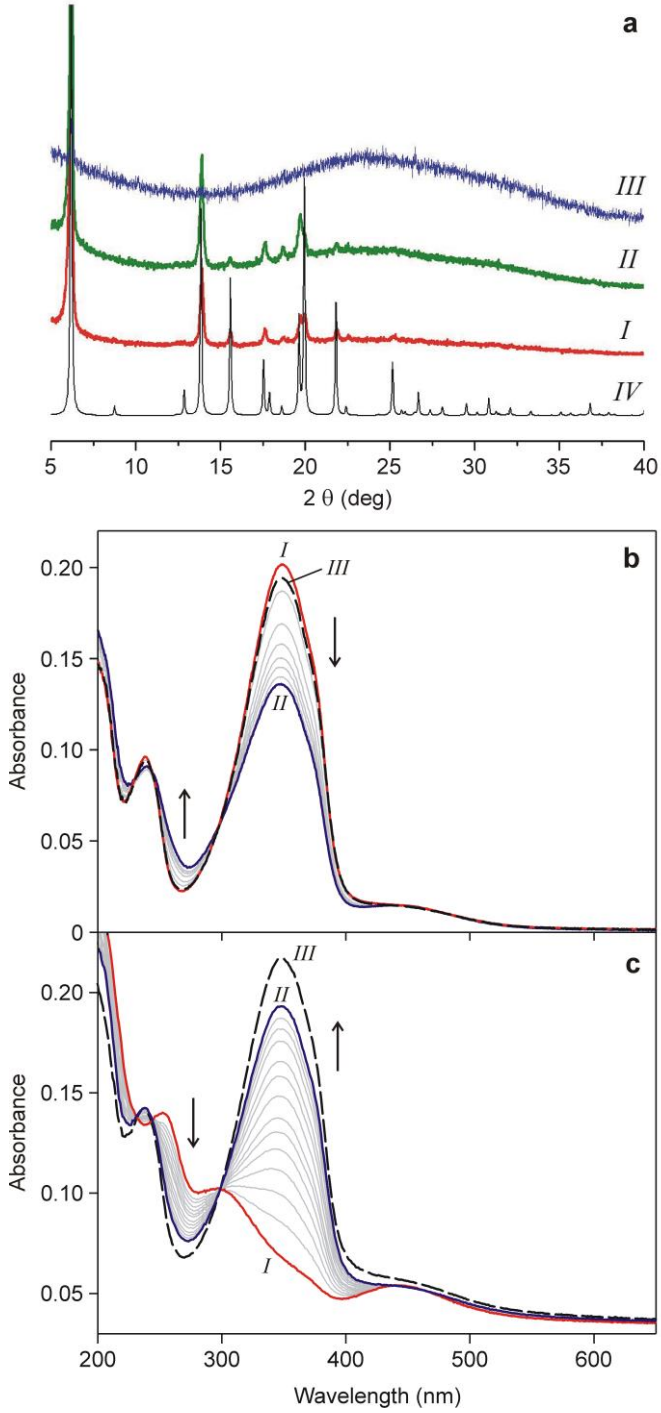

Fig. 3 | Observation of the photoisomerization of 1c in a thin solid film by XRPD and UV-vis absorption spectroscopy. (a) XRPD patterns obtained before (*I*) and after 48 h (*II*) and 96 h (*III*) of irradiation of a drop casted film of E_4-**1c** at 365 nm; the pattern calculated on the basis of single crystal data (*IV*) is also shown (for sake of clarity all patterns are expanded vertically). (b) Absorption spectra of a spin coated thin film of E_4-**1c** before (*I*) and after (*II*) irradiation at 365 nm for 6 min (photostationary state); spectra taken at intermediate times are shown in light grey. Curve *III* is the spectrum obtained after heating the film at 130 °C for 10 min. (c) Absorption spectrum of a Z_4-**1c** thin film before (*I*) and after (*II*) irradiation at 436 nm for 34 min (photostationary state); spectra taken at intermediate times are shown in light grey. Curve *III* (dashed line) is the spectrum obtained after heating the film at 130 °C for 10 min.

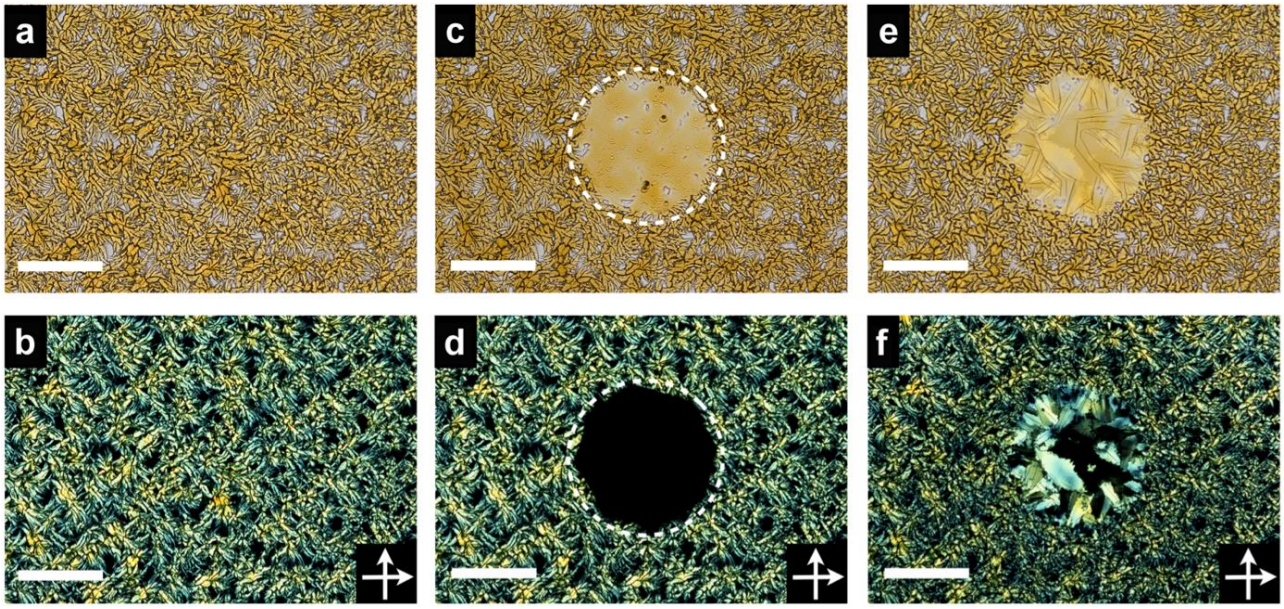

Fig. 4 | Effect of photochemical and thermal stimulation on the 1c crystals. Polarizing optical photomicrographs of solid E_4-**1c** under bright field (top) and cross-polarized (bottom) light illumination, before (a, b) and after (c, d) near-UV irradiation (330-380 nm) in a central spot (dashed line) for 10 min. (e, f) Recrystallization of the irradiated sample is observed upon thermal annealing at 160 °C for 20 min. Scale bar is 100 μm.

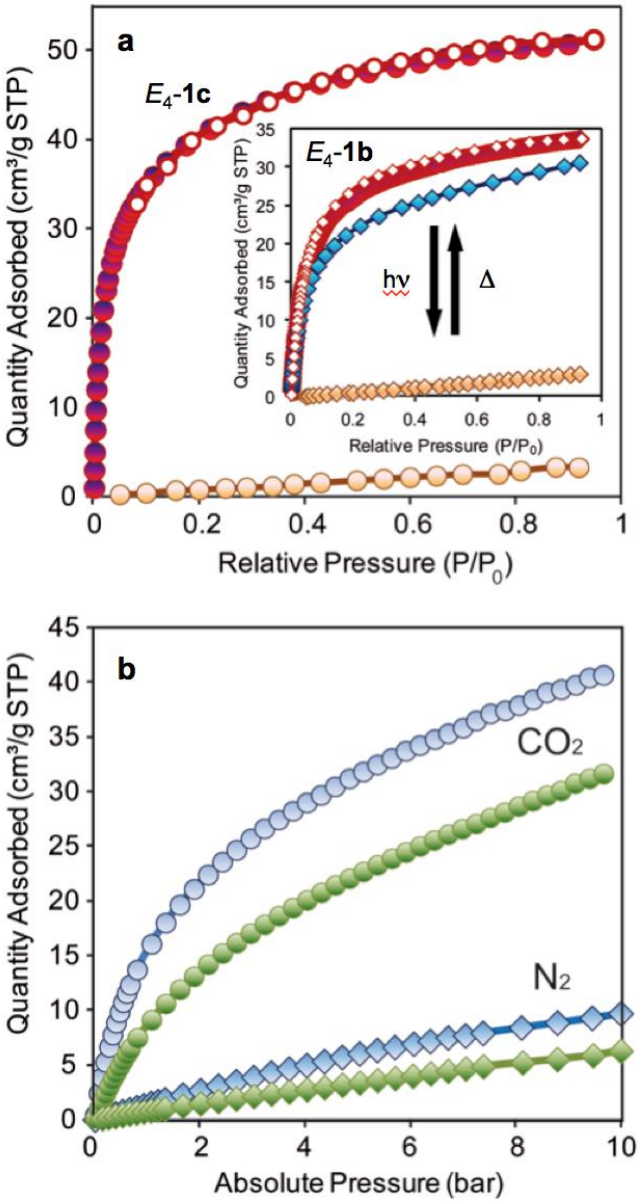

Fig. 5 | Switching of gas adsorption properties and observation of CO_2/N_2 selectivity. (a) CO_2 adsorption isotherms of E_4-**1c** (red circles) and Z_4-**1c** (orange circles) at 195 K. The inset shows the CO_2 adsorption isotherms at 195 K of E_4-**1b** (red diamonds), Z_4-**1b** (orange diamonds), and the Z_4-**1b** sample after heating at 160 °C for 2 hours (blue diamonds). (b) CO_2 (circles) and N_2 (diamonds) adsorption isotherms of E_4-**1c** at 298 K (green) and 273 K (blue).